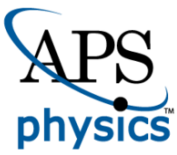

Heating Rates in Periodically Driven Strongly Interacting Quantum Many-Body Systems

Krishnanand Mallayya and Marcos Rigol

Phys. Rev. Lett. **123**, 240603 — Published 12 December 2019

DOI: 10.1103/PhysRevLett.123.240603

Heating rates in periodically driven strongly interacting quantum many-body systems

Krishnanand Mallayya and Marcos Rigol
Department of Physics, The Pennsylvania State University, University Park, PA 16802, USA

We study heating rates in strongly interacting quantum lattice systems in the thermodynamic limit. Using a numerical linked cluster expansion, we calculate the energy as a function of the driving time and find a robust exponential regime. The heating rates are shown to be in excellent agreement with Fermi's golden rule. We discuss the relationship between heating rates and, within the eigenstate thermalization hypothesis, the smooth function that characterizes the off-diagonal matrix elements of the drive operator in the eigenbasis of the static Hamiltonian. We show that such a function, in nonintegrable and (remarkably) integrable Hamiltonians, can be probed experimentally by studying heating rates as functions of the drive frequency.

PACS numbers: 02.30.Lt, 02.60.-x, 05.30.Jp, 05.70.Ln, 75.10.Jm

Periodic perturbations are a ubiquitous tool to excite and probe quantum systems and study their response functions. Recent developments in theory and experiments have expanded the scope of periodic driving to generate effective magnetic fields [1–4], as well as to engineer topologically non-trivial band structures [5–8] and novel time-crystalline phases [9–14]. However, under periodic driving, generic many-body interacting systems are expected to heat up and (for a bounded spectrum, typical of lattice fermions and spins) equilibrate at long times to states that are effectively at infinite temperature [15, 16].

Driving at high frequencies, because of prethermalization [17–30], has been proposed to slow down heating [10, 31–34]. It results in initial fast pre-thermal dynamics towards time-periodic steady states (prethermal states) of effective local Hamiltonians [35–38], before thermalization dynamics eventually results in featureless "infinite-temperature" states [15, 16, 39, 40]. Prethermalization is a universal phenomenon that occurs during dynamics in isolated [30] and open [27, 28] systems whenever conservation laws are weakly broken. Numerical studies of prethermalization and thermalization, or, in general, of energy absorption in driven strongly interacting systems with many particles (or spins) are challenging. Progress has been achieved using massively parallel Krylov subspace methods [32], density matrix truncation [41], and t-DMRG [42], but there is a dearth of computational techniques to study generic models in arbitrary dimensions.

Here, we report on the implementation of a numerical linked cluster expansion (NLCE) for driven systems. NLCEs can be used to study arbitrary interaction strengths in arbitrary dimensions. They were originally introduced to study thermal equilibrium ensembles [43], where they outperform full exact diagonalization calculations [44]. NLCEs were recently implemented to study thermalization [45] and quantum dynamics under time-independent Hamiltonians in one [30, 46] and two [47, 48] dimensions, and combined with dynamical quantum typicality [49]. We use them to determine heating rates in strongly interacting one-dimensional (1D) lattices in the thermodynamic limit. The numerically obtained rates are shown to agree with Fermi's golden rule predictions. We argue that, in addition to helping quantify the stability of prethermal states, heating rates can be used to probe the structure of the off-diagonal matrix elements of the drive operator in the eigenstates of the static Hamiltonian.

We consider a time-periodic Hamiltonian of the form $\hat{H}(\tau) = \hat{H}_0 + g(\tau)\hat{K}$, where $\hat{H}_0$ is the static Hamiltonian and $g(\tau)\hat{K}$ is a weak time-periodic perturbation of strength g, period $T = 2\pi/\Omega$, and zero time average. The system is initialized (at $\tau = 0$) in a state $\hat{\rho}_I = \exp[-\beta_I \hat{H}_I]/\mathrm{Tr}\{\exp[-\beta_I \hat{H}_I]\}$ that is a thermal equilibrium state of an initial static Hamiltonian $\hat{H}_I$ at an inverse temperature β_I. At stroboscopic times $\tau = nT$ $(n = 0, 1, 2, \dots)$, the density matrix $\hat{\rho}(\tau)$ can be written as $\hat{\rho}(\tau) = (\hat{U}_F)^n \hat{\rho}_I (\hat{U}_F^\dagger)^n$, where $\hat{U}_F = \mathcal{T}\exp[-i\int_0^T \hat{H}(t)dt]$ is the (time ordered $\mathcal{T}$) Floquet evolution operator (we set $\hbar = 1$). We assume that $\hat{H}_I$, $\hat{H}_0$, and $\hat{K}$ are translationally invariant sums of local operators, and that they are mutually noncommuting (nontrivial dynamics occurs even if $g = 0$).

The obvious conservation law broken by $g(\tau)\hat{K}$ is energy conservation. For sufficiently small g in the thermodynamic limit, we expect prethermalization to occur (independently of the value of Ω), wherein the system quickly relaxes to the equilibrium state of $\hat{H}_0$ described by a (generalized) Gibbs ensemble [up to $O(g)$ corrections]. The relaxation towards "infinite temperature" can be described by a slowly evolving (generalized) Gibbs ensemble of $\hat{H}_0$, characterized by the instantaneous expectation values of the conserved quantities of $\hat{H}_0$ [30]. The dynamics of those quantities is described by autonomous equations, with drifts given by Fermi's golden rule [30].

We study the evolution of the energy defined by the static Hamiltonian, which is also the time-averaged Hamiltonian $\overline{\hat{H}(\tau)} = \hat{H}_0$, $E(\tau) = \mathrm{Tr}[\hat{H}_0\hat{\rho}(\tau)]$. We consider general time-periodic perturbations, which can be Fourier decomposed as $g(\tau)\hat{K} = \sum_{m>0} 2g_m \sin(m\Omega\tau)\hat{K}$. After a short initial transient dynamics, in the linear response regime, the system absorbs energy independently

from each Fourier mode m. The average rate of energy absorption over a cycle is $\dot{E}(\tau) = \sum_{m>0} \dot{E}_m(\tau)$ with, as expected from Fermi's golden rule,

$$\dot{E}_m(\tau) = 2\pi g_m^2 \sum_{i,f} |\langle E_f^0|\hat{K}|E_i^0\rangle|^2 (E_f^0 - E_i^0) P_i^0(\tau) \times \delta(E_f^0 - E_i^0 \pm m\Omega), \quad (1)$$

where $|E_i^0\rangle$ ($|E_f^0\rangle$) are the eigenkets of $\hat{H}_0$ with eigenenergies E_i^0 (E_f^0), and $P_i^0(\tau) = \langle E_i^0|\hat{\rho}(\tau)|E_i^0\rangle$ is the projection of $\hat{\rho}(\tau)$ into the basis of $\hat{H}_0$. The latter defines the so-called diagonal ensemble (DE) at time τ [50], $\hat{\rho}_{\rm DE}(\tau) = P_i^0(\tau)|E_i^0\rangle\langle E_i^0|$. $\hat{\rho}_{\rm DE}(\tau)$ is expected to characterize the equilibrated state under $\hat{H}_0$ at time τ [51]. We define the rate $\Gamma(\tau) = \sum_{m>0} \Gamma_m(\tau)$, where $\Gamma_m(\tau) = \dot{E}_m(\tau)/[E_\infty - E(\tau)]$ is the rate for Fourier mode m, and E_∞ is the energy at infinite temperature. Only when sufficiently small is that one expects $|E_\infty - E(\tau)|$ to be an exponential function, and $\Gamma(\tau)$ to be meaningful.

We focus on 1D lattice system of hard-core bosons, with $\hat{H}_0$ and $\hat{K}$ given by

$$\hat{H}_0 = \sum_i \Big[\Big(-t\,\hat{b}_i^\dagger \hat{b}_{i+1} - t'\,\hat{b}_i^\dagger \hat{b}_{i+2} + h\,\hat{b}_i^\dagger\Big) + \text{H.c.} + V\left(\hat{n}_i - \frac{1}{2}\right)\left(\hat{n}_{i+1} - \frac{1}{2}\right) + V'\left(\hat{n}_i - \frac{1}{2}\right)\left(\hat{n}_{i+2} - \frac{1}{2}\right)\Big], \quad (2)$$

$$\hat{K} = -\sum_i \left(\hat{b}_i^\dagger \hat{b}_{i+1} + \text{H.c.}\right), \quad (3)$$

where standard notation was used [52]. We drive the system with a square wave $g(\tau) = g\,\text{sgn}[\sin(\Omega\tau)]$, and set $t = V = 1$ (our unit of energy and frequency). $\hat{H}_0$ is integrable for $t' = V' = h = 0$ (and mappable to the spin-1/2 XXZ Hamiltonian [52]), and nonintegrable for nonvanishing t', V', and h. We study integrable and nonintegrable (with $t' = V' = 0.8$ and $h = 1.0$) cases, and select $\hat{H}_I$ to have the same terms as $\hat{H}_0$ [Eq. (2)] but with different nearest neighbor coupling parameters ($t_I = 0.5$ and $V_I = 2.0$).

We implement a NLCE to calculate the energy per site $e(\tau) = E(\tau)/L$ at stroboscopic times in the thermodynamic limit ($L \to \infty$). Within NLCEs, $e(\tau)$ is expressed as a sum over the contributions of all connected clusters (c) that can be embedded on the lattice, $e(\tau) = \sum_c M(c) \times W_c^e(\tau)$, where $M(c)$ is the number of "embeddings" (per site) of cluster c, and $W_c^e(\tau)$ is the weight of $e(\tau)$ in cluster c. $W_c^e(\tau)$ is obtained recursively using the inclusion-exclusion principle: $W_c^e(\tau) = E_c(\tau) - \sum_{c'\subset c} W_{c'}^e(\tau)$, where c' denotes the connected sub-clusters of c and $E_c(\tau) = \text{Tr}[\hat{H}_0^c \hat{\rho}_c(\tau)]$ is the energy in cluster c [$\hat{H}_0^c$ is the static Hamiltonian, and $\hat{\rho}_c(\tau)$ is the density matrix at time τ, both in cluster c]. The series starts with the smallest cluster (a site) for which $W_c(\tau) = E_c(\tau)$. For each cluster, $E_c(\tau)$ is calculated numerically using full exact diagonalization. We use maximally connected clusters (clusters with contiguous sites and all possible bonds) as they are optimal to study dynamics in chains in the presence of nearest and next-nearest neighbor interactions [45, 46, 54]. The order of the NLCE is set by the number of sites of the largest cluster considered. For nonintegrable $\hat{H}_0$, we compute 17 orders of the NLCE (after exploiting all symmetries, the dimension of largest sector of the Hamiltonian is 32,896). When $\hat{H}_0$ is integrable, due to particle number conserva-

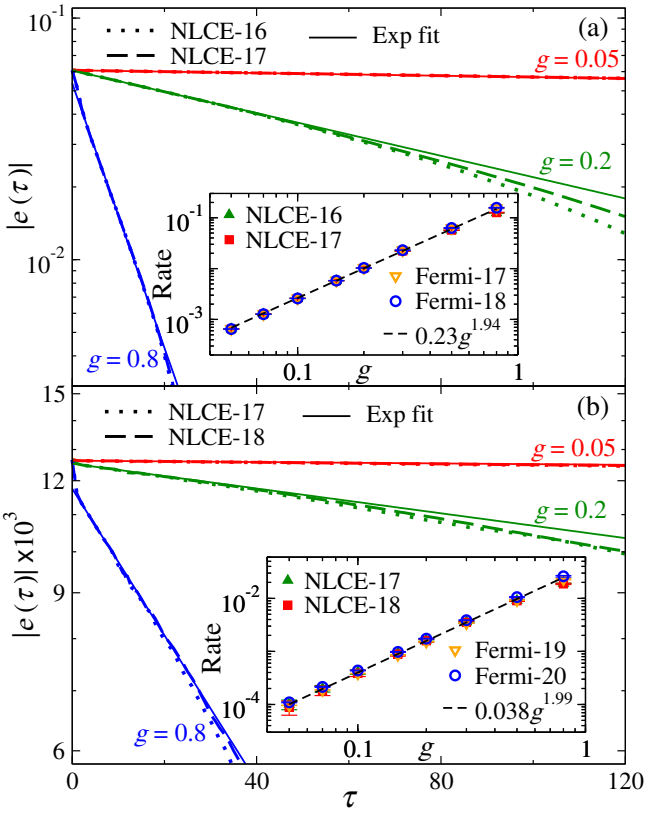

FIG. 1. (Main panels) Absolute value of the energy per site $|e(\tau)|$ vs τ for (a) the nonintegrable and (b) the integrable $\hat{H}_0$ for three strengths $g = \{0.05, 0.2, 0.8\}$ of the drive, a period $T = 1.0$, and $\beta_I = (30)^{-1}$. Results (at stroboscopic times) are obtained using NLCE to: (a) 16 (NLCE-16) and 17 (NLCE-17) orders, and (b) 17 (NLCE-17) and 18 (NLCE-18) orders. The solid lines show exponential fits to the highest NLCE order. (Insets) Rates obtained in fits, as those depicted in the main panels, for the two highest NLCE orders. For all values of g, the fits for the nonintegrable $\hat{H}_0$ are done for times $3 \le \tau \le 20$ for NLCE-17 and $3 \le \tau \le 15$ for NLCE-16, while for the integrable $\hat{H}_0$ they are done for times $2 \le \tau \le 8$ for NLCE-18 and $2 \le \tau \le 7$ for NLCE-17. The Fermi golden rule predictions (open symbols) are evaluated using full exact diagonalization in chains with: (a) 17 and 18 sites (Fermi-17 and Fermi-18) and (b) 19 and 20 sites (Fermi-19 and Fermi-20), and periodic boundary conditions. Errorbars indicate the fitting errors for the NLCE rates, and the standard deviation from averages over different values of ΔE and τ for the Fermi golden rule predictions [53]. Power-law fits (αg^γ) of the rates in both insets are done for the highest order of the NLCE in the interval $0.05 \le g \le 0.3$.

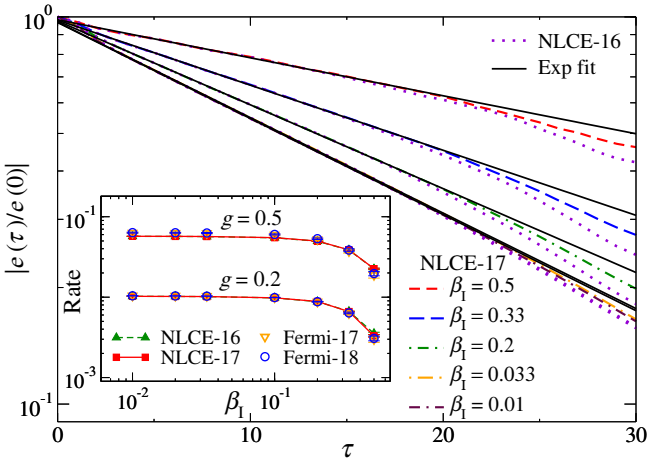

FIG. 2. (Main panel) Absolute value of the energy per site $|e(\tau)|$, normalized by its initial value $|e(0)|$, for a periodically driven nonintegrable $\hat{H}_0$ with $g = 0.5$ and $T = 1.0$, for initial thermal states of $\hat{H}_I$ at different inverse temperatures β_I. We show results for 16 and 17 orders of the NLCE (NLCE-16 and NLCE-17, respectively), and exponential fits to the NLCE-17 results. (Inset) Rates obtained from exponential fits to NLCE-17 for $3 \leq \tau \leq 20$ (as those in the main panel) and NLCE-16 for $3 \leq \tau \leq 15$ vs β_I, for $g = 0.2$ and $g = 0.5$. We also report Fermi's golden rule predictions obtained using full exact diagonalization in chains with 17 and 18 sites (Fermi-17 and Fermi-18) and periodic boundary conditions.

tion, we are able to compute 18 orders of the NLCE (the dimension of the largest sector in this case is 21,942).

In the main panels of Fig. 1, we show NLCE results for $|e(\tau)|$ vs τ for (a) the nonintegrable and (b) the integrable static Hamiltonians, for three strengths $g = 0.05$, 0.2, and 0.8 of the drive, for an initial thermal equilibrium state of $\hat{H}_I$ at an inverse temperature $\beta_I = (30)^{-1}$. The exponential fits, which exclude the short-time transient dynamics and long times at which the NLCE does not converge, make apparent that the approach of $e(\tau)$ to the infinite temperature energy ($E_\infty/L = 0$) is exponential. The rates obtained from such fits are plotted in the insets of Fig. 1 vs g, for the two highest orders of the NLCE. They agree with each other, indicating that the fits are robust. The rates are $\propto g^2$ and are in excellent agreement with Fermi's golden rule [Eq. (1)], evaluated numerically using full exact diagonalization in chains with periodic boundary conditions [53].

It follows from eigenstate thermalization for nonintegrable Hamiltonians [50, 51, 55, 56] (generalized eigenstate thermalization for integrable Hamiltonians [57, 58]) $\hat{H}_0$ that the predictions of $\hat{\rho}_{\rm DE}(\tau)$ for few-body operators agree with those of the thermal (generalized Gibbs) ensemble [51, 58–60]. We first focus on the case in which $\hat{H}_0$ is nonintegrable with no local conservation law. In this case, the inverse temperature $\beta(\tau)$ alone characterizes the thermal (grand canonical) ensemble at τ, $\hat{\rho}_{\rm GE}(\tau) = \exp[-\beta(\tau)\hat{H}_0]/{\rm Tr}\{\exp[-\beta(\tau)\hat{H}_0]\}$, where $\beta(\tau)$ is determined by the condition ${\rm Tr}[\hat{H}_0\hat{\rho}_{\rm GE}(\tau)] = {\rm Tr}[\hat{H}_0\hat{\rho}(\tau)]$. Only when $\beta(\tau) \ll 1$ is that one expects $\Gamma(\tau)$ to become independent of $\beta(\tau)$, and $E(\tau)$ to approach E_∞ as a single exponential.

To illustrate this, in the main panel of Fig. 2 we plot $|e(\tau)|$ (normalized by its initial value $|e(0)|$) for various initial inverse temperatures $\beta_I \in [0.01, 0.5]$. The normalized energies $e(\tau)/e(0)$ for $\beta_I = 0.033$ and 0.01 exhibit a nearly identical exponential decay (within the times at which the NLCE has converged) implying that Γ is independent of β_I [hence, of $\beta(\tau)$] when $\beta_I \lesssim 0.03$. For $\beta_I \gtrsim 0.2$, one can still use exponentials to fit $e(\tau)$, but the rates obtained depend on β_I. In the inset in Fig. 2, we report the rates obtained from such fits vs β_I using two orders of the NLCE and for two values of g. The rates from the two orders of the NLCE agree with each other and agree well with Fermi's golden rule predictions. (Worse agreement is seen for $g = 0.5$ than for $g = 0.2$ due to the effect of higher order corrections.) The increase in the rate seen in the inset in Fig. 2 with decreasing β_I is the one expected to occur as a function of driving time for initial states that are not in the regime $\beta_I \ll 1$.

Next we focus on the dependence of the heating rates on Ω. In nonintegrable systems, the eigenstate thermalization hypothesis (ETH) [50, 51, 55, 56] allows one to compute $\Gamma_m(\tau)$. After resolving all symmetries of the static Hamiltonian, the ETH ansatz for the matrix elements $K^{(s)}_{i,f} = \langle E^0_i|\hat{K}|E^0_f\rangle$ of the operator $\hat{K}$ (used as drive) in each block diagonal sector s of $\hat{H}_0$ has the form [51, 61]

$$K^{(s)}_{i,f} = K^{(s)}(E)\delta_{i,f} + [D^{(s)}(E)]^{-1/2} f^{(s)}_K(E,\omega) R_{i,f}, \quad (4)$$

where $E = (E_i + E_f)/2$, $\omega = E_f - E_i$, $D^{(s)}(E)$ is the density of states of $\hat{H}_0$ in sector s at energy E, and $R_{i,f}$ is a random variable with zero mean and unit variance. $K^{(s)}(E)$ and $f^{(s)}_K(E,\omega)$ are smooth functions of their arguments.

Using Eqs. (1) and (4), changing sums over eigenstates by integrals over energy, replacing $\hat{\rho}_{\rm DE}(\tau)$ by $\hat{\rho}_{\rm GE}(\tau)$ and assuming high temperature [$\beta(\tau) \ll 1$], one obtains the following expression for the heating rate [53]

$$\Gamma_m = \frac{2\pi(m\Omega g_m)^2}{{\rm Tr}(\hat{H}_0^2)} \sum_s \int_{E^{(s)}_{\rm min}+m\Omega/2}^{E^{(s)}_{\rm max}-m\Omega/2} dE\, |f^{(s)}_K(E, m\Omega)|^2 \times D^{(s)}(E + m\Omega/2) D^{(s)}(E - m\Omega/2)/D^{(s)}(E), \quad (5)$$

where $E^{(s)}_{\rm min}$ ($E^{(s)}_{\rm max}$) is the minimum (maximum) energy in sector s, and $m\Omega$ is smaller than $E^{(s)}_{\rm max} - E^{(s)}_{\rm min}$ (otherwise there is no linear response heating for that mode).

In Fig. 3(a), we compare heating rates (for the nonintegrable case and normalized by g^2) obtained from dynamics evaluated with NLCE (see inset) and the ones predicted by Eq. (5) [53]. NLCE results are not reported for small and large values of Ω because the time interval

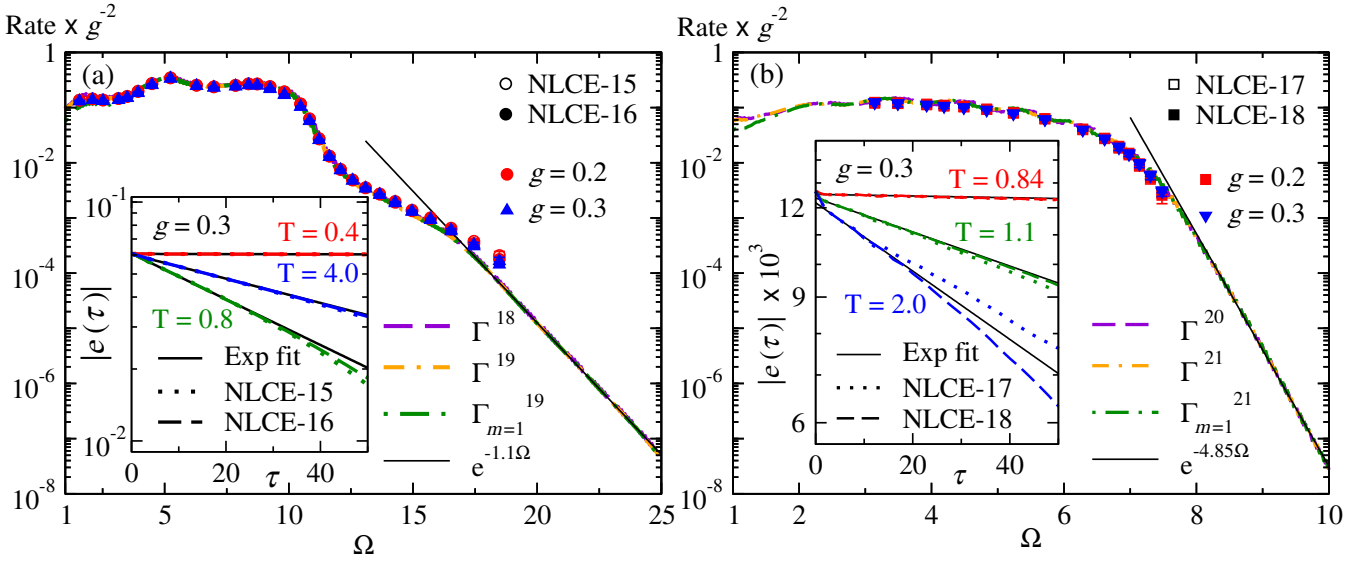

FIG. 3. (Main panels) Heating rates (normalized by g^2) vs Ω for (a) the nonintegrable and (b) the integrable $\hat{H}_0$, for $g = 0.2$ and $g = 0.3$. Rates obtained from exponential fits of the dynamics (as in the insets) are shown as symbols for NLCE to (a) 15 (NLCE-15) and 16 (NLCE-16) orders, and (b) to 17 (NLCE-17) and 18 (NLCE-18) orders. Rates obtained from Eq. (5) evaluated using full exact diagonalization in periodic chains are shown as lines for (a) 18 (Γ^{18}) and 19 (Γ^{19}) sites, and (b) 20 (Γ^{20}) and 21 (Γ^{21}) sites. We also show rates of the Fourier mode $m = 1$ in Eq. (5) for (a) 19 [$\Gamma^{19}_{m=1}$] and (b) 21 [$\Gamma^{21}_{m=1}$] sites, as well as exponential fits of the results at high Ω. (Insets) Absolute value of the energy per site $|e(\tau)|$ vs τ, using NLCE to (a) 15 (NLCE-15) and 16 (NLCE-16) orders and (b) 17 (NLCE-17) and 18 (NLCE-18) orders, for $g = 0.3$ and three different driving periods $T = 2\pi/\Omega$. Exponential fits to the highest order of the NLCE are shown as solid lines. The rates reported in the main panels are obtained from exponential fits for (a) $3 \leq \tau \leq 15$ for NLCE-16 and $3 \leq \tau \leq 12$ for NLCE-15, and (b) $2 \leq \tau \leq 8$ for NLCE-18 and $2 \leq \tau \leq 7.5$ for NLCE-17, for all g and T (errorbars indicate fitting errors).

in which the NLCE converges is not sufficiently long to produce robust exponential fits. The normalized rates for $g = 0.2$ and $g = 0.3$ are nearly identical to one another, and are well described by Eq. (5). For high Ω, we find that the evaluation of Eq. (5) results in heating rates that can be well described by an exponential in Ω. This is consistent with rigorous bounds [10, 31, 36].

When $\hat{H}_0$ is integrable (the spin-1/2 XXZ limit), the prethermal states are described by a generalized Gibbs ensemble (GGE) $\hat{\rho}_{\rm GGE}(\tau)$ [62–64]. When $\hat{\rho}_I$ is a thermal state with $\beta_I \ll 1$ (or in general after long driving times), $\hat{\rho}_{\rm GGE}(\tau) \simeq \hat{\rho}_{\rm GE}(\tau)$ with $\beta(\tau) \ll 1$ [65]. In this regime, Eq. (5) gives the heating rates for the integrable static Hamiltonian provided that there is a well defined $|f_K^{(s)}(E,\omega)|^2$. In Fig. 3(b), we show the equivalent of Fig. 3(a) but for the integrable case. Despite the differences between the dependence of the heating rates on Ω in the nonintegrable and integrable cases, the heating rates in the latter are described by Eq. (5) and, for high Ω, they are well described by an exponential in Ω.

The previous results show that heating rates can be used to probe the function $f_K^{(s)}(E, m\Omega)$ in nonintegrable and integrable systems. Still, Eq. (4) involves the density of states. For large systems sizes, since E is extensive but Ω is not: $D^{(s)}(E + m\Omega/2)D^{(s)}(E - m\Omega/2) \simeq [D^{(s)}(E)]^2$ and $E^{(s)}_{\rm min,max} \pm m\Omega/2 \simeq E^{(s)}_{\rm min,max}$. Using the saddle point approximation to compute the integral in Eq. (5), and using that $D^{(s)}(E_\infty)$ is maximal, the heating rate for Fourier mode m in the thermodynamic limit (Γ^∞_m) can be written as

$$\Gamma^\infty_m = \frac{2\pi(m\Omega g_m)^2}{{\rm Tr}(\hat{H}_0^2)} \sum_s |f_K^{(s)}(E_\infty, m\Omega)|^2 Z(s), \quad (6)$$

where $Z(s)$ is the Hilbert space dimension of sector s. Thus the rate for Fourier mode $m = 1$, which Fig. 4 shows to be in excellent agreement with the heating rates obtained from the NLCE dynamics for a wide range of values of Ω, gives the average $|f_K^{(s)}(E_\infty, \Omega)|^2$ over all sectors of the Hamiltonian in the thermodynamic limit [53].

In summary, we studied heating in strongly interacting driven lattice systems and showed that, at sufficiently high effective temperatures ($[\beta(\tau)]^{-1} \gtrsim 2$), it can be well characterized by rates no matter whether the system is nonintegrable or integrable. We also showed that the rates agree with Fermi's golden rule predictions for both nonintegrable or integrable cases. We then argued that heating rates can be used to probe the structure of off-diagonal matrix elements of the operator used to drive the system, in the eigenstates of the static Hamiltonian. Our results suggest that there is a well defined $|f_K^{(s)}(E, \Omega)|^2$ in integrable interacting systems. This has been confirmed in a recent full exact diagonalization study of the spin-1/2 XXZ chain [66], and needs to be

further explored to place it on equal footing with what is known for quantum chaotic systems [51, 67–72].

This work was supported by the National Science Foundation under Grant No. PHY-1707482. We are grateful to W. De Roeck and S. Gopalakrishnan for motivating discussions. The computations were carried out at the Institute for CyberScience at Penn State.

[1] J. Dalibard, F. Gerbier, G. Juzeliūnas, and P. Öhberg, Rev. Mod. Phys. **83**, 1523 (2011).
[2] T. Kitagawa, T. Oka, A. Brataas, L. Fu, and E. Demler, Phys. Rev. B **84**, 235108 (2011).
[3] M. Aidelsburger, M. Atala, M. Lohse, J. T. Barreiro, B. Paredes, and I. Bloch, Phys. Rev. Lett. **111**, 185301 (2013).
[4] N. Goldman, G. Juzeliūnas, P. Öhberg, and I. B. Spielman, Rep. Prog. Phys. **77**, 126401 (2014).
[5] T. Oka and H. Aoki, Phys. Rev. B **79**, 081406(R) (2009).
[6] N. H. Lindner, G. Refael, and V. Galitski, Nature Phys. **7**, 490 (2011).
[7] M. C. Rechtsman, J. M. Zeuner, Y. Plotnik, Y. Lumer, D. Podolsky, F. Dreisow, S. Nolte, M. Segev, and A. Szameit, Nature **496**, 196 (2013).
[8] N. R. Cooper, J. Dalibard, and I. B. Spielman, Rev. Mod. Phys. **91**, 015005 (2019).
[9] D. V. Else, B. Bauer, and C. Nayak, Phys. Rev. Lett. **117**, 090402 (2016).
[10] D. V. Else, B. Bauer, and C. Nayak, Phys. Rev. X **7**, 011026 (2017).
[11] V. Khemani, A. Lazarides, R. Moessner, and S. L. Sondhi, Phys. Rev. Lett. **116**, 250401 (2016).
[12] N. Y. Yao, A. C. Potter, I.-D. Potirniche, and A. Vishwanath, Phys. Rev. Lett. **118**, 030401 (2017); Phys. Rev. Lett. **118**, 269901(E) (2017).
[13] J. Zhang, P. Hess, A. Kyprianidis, P. Becker, A. Lee, J. Smith, G. Pagano, I.-D. Potirniche, A. C. Potter, A. Vishwanath, *et al.*, Nature **543**, 217 (2017).
[14] S. Choi, J. Choi, R. Landig, G. Kucsko, H. Zhou, J. Isoya, F. Jelezko, S. Onoda, H. Sumiya, V. Khemani, *et al.*, Nature **543**, 221 (2017).
[15] L. D'Alessio and M. Rigol, Phys. Rev. X **4**, 041048 (2014).
[16] A. Lazarides, A. Das, and R. Moessner, Phys. Rev. E **90**, 012110 (2014).
[17] M. Moeckel and S. Kehrein, Phys. Rev. Lett. **100**, 175702 (2008); Ann. Phys. **324**, 2146 (2009).
[18] M. Eckstein, M. Kollar, and P. Werner, Phys. Rev. Lett. **103**, 056403 (2009).
[19] M. Kollar, F. A. Wolf, and M. Eckstein, Phys. Rev. B **84**, 054304 (2011).
[20] M. Tavora and A. Mitra, Phys. Rev. B **88**, 115144 (2013).
[21] M. Tavora, A. Rosch, and A. Mitra, Phys. Rev. Lett. **113**, 010601 (2014).
[22] N. Nessi, A. Iucci, and M. A. Cazalilla, Phys. Rev. Lett. **113**, 210402 (2014).
[23] F. H. L. Essler, S. Kehrein, S. R. Manmana, and N. J. Robinson, Phys. Rev. B **89**, 165104 (2014).
[24] B. Bertini, F. H. L. Essler, S. Groha, and N. J. Robinson, Phys. Rev. Lett. **115**, 180601 (2015); Phys. Rev. B **94**, 245117 (2016).
[25] E. Canovi, M. Kollar, and M. Eckstein, Phys. Rev. E **93**, 012130 (2016).
[26] M. Fagotti and M. Collura, arXiv:1507.02678.
[27] F. Lange, Z. Lenarčič, and A. Rosch, Phys. Rev. B **97**, 165138 (2018).
[28] Z. Lenarčič, F. Lange, and A. Rosch, Phys. Rev. B **97**, 024302 (2018).
[29] P. Reimann and L. Dabelow, Phys. Rev. Lett. **122**, 080603 (2019).
[30] K. Mallayya, M. Rigol, and W. De Roeck, Phys. Rev. X **9**, 021027 (2019).
[31] D. A. Abanin, W. De Roeck, and F. Huveneers, Phys. Rev. Lett. **115**, 256803 (2015).
[32] F. Machado, G. D. Meyer, D. V. Else, C. Nayak, and N. Y. Yao, arXiv:1708.01620 (2017).
[33] S. A. Weidinger and M. Knap, Sci. Rep. **7**, 45382 (2017).
[34] C. Kuhlenkamp and M. Knap, arXiv:1906.06341.
[35] D. A. Abanin, W. De Roeck, W. W. Ho, and F. Huveneers, Phys. Rev. B **95**, 014112 (2017).
[36] D. Abanin, W. De Roeck, W. W. Ho, and F. Huveneers, Commun. Math. Phys **354**, 809 (2017).
[37] T. Mori, T. Kuwahara, and K. Saito, Phys. Rev. Lett. **116**, 120401 (2016).
[38] T. Kuwahara, T. Mori, and K. Saito, Ann. Phys. (N. Y.) **367**, 96 (2016).
[39] T. Prosen, Phys. Rev. Lett. **80**, 1808 (1998).
[40] L. DAlessio and A. Polkovnikov, Ann. Phys. **333**, 19 (2013).
[41] B. Ye, F. Machado, C. D. White, R. S. Mong, and N. Y. Yao, arXiv:1902.01859 (2019).
[42] C. Kollath, A. Iucci, T. Giamarchi, W. Hofstetter, and U. Schollwöck, Phys. Rev. Lett. **97**, 050402 (2006).
[43] M. Rigol, T. Bryant, and R. R. P. Singh, Phys. Rev. Lett. **97**, 187202 (2006); Phys. Rev. E **75**, 061118 (2007); Phys. Rev. E **75**, 061119 (2007).
[44] D. Iyer, M. Srednicki, and M. Rigol, Phys. Rev. E **91**, 062142 (2015).
[45] M. Rigol, Phys. Rev. Lett. **112**, 170601 (2014); Phys. Rev. Lett. **116**, 100601 (2016).
[46] K. Mallayya and M. Rigol, Phys. Rev. Lett. **120**, 070603 (2018).
[47] I. G. White, B. Sundar, and K. R. Hazzard, arXiv:1710.07696 (2017).
[48] E. Guardado-Sanchez, P. T. Brown, D. Mitra, T. Devakul, D. A. Huse, P. Schauß, and W. S. Bakr, Phys. Rev. X **8**, 021069 (2018).
[49] J. Richter and R. Steinigeweg, Phys. Rev. B **99**, 094419 (2019).
[50] M. Rigol, V. Dunjko, and M. Olshanii, Nature **452**, 854 (2008).
[51] L. D'Alessio, Y. Kafri, A. Polkovnikov, and M. Rigol, Adv. Phys. **65**, 239 (2016).
[52] M. A. Cazalilla, R. Citro, T. Giamarchi, E. Orignac, and M. Rigol, Rev. Mod. Phys. **83**, 1405 (2011).
[53] See Supplemental Material for the details on the numerical evaluation of Eqs. (1) and (5), on the derivation of Eq. (5), for results from the evaluation of Eq. (6), and for a discussion of the convergence of the NLCE and exact diagonalization calculations.
[54] K. Mallayya and M. Rigol, Phys. Rev. E **95**, 033302 (2017).
[55] J. M. Deutsch, Phys. Rev. A **43**, 2046 (1991).
[56] M. Srednicki, Phys. Rev. E **50**, 888 (1994).

[57] A. C. Cassidy, C. W. Clark, and M. Rigol, Phys. Rev. Lett. **106**, 140405 (2011).
[58] L. Vidmar and M. Rigol, J. Stat. Mech., 064007 (2016).
[59] F. H. L. Essler and M. Fagotti, J. Stat. Mech., 064002 (2016).
[60] J.-S. Caux, J. Stat. Mech., 064006 (2016).
[61] M. Srednicki, J. Phys. A **32**, 1163 (1999).
[62] B. Wouters, J. De Nardis, M. Brockmann, D. Fioretto, M. Rigol, and J.-S. Caux, Phys. Rev. Lett. **113**, 117202 (2014).
[63] B. Pozsgay, M. Mestyán, M. A. Werner, M. Kormos, G. Zaránd, and G. Takács, Phys. Rev. Lett. **113**, 117203 (2014).
[64] E. Ilievski, J. De Nardis, B. Wouters, J.-S. Caux, F. H. L. Essler, and T. Prosen, Phys. Rev. Lett. **115**, 157201 (2015).
[65] K. He and M. Rigol, Phys. Rev. A **85**, 063609 (2012).
[66] T. LeBlond et al., in preparation.
[67] E. Khatami, G. Pupillo, M. Srednicki, and M. Rigol, Phys. Rev. Lett. **111**, 050403 (2013).
[68] R. Steinigeweg, J. Herbrych, and P. Prelovšek, Phys. Rev. E **87**, 012118 (2013).
[69] W. Beugeling, R. Moessner, and M. Haque, Phys. Rev. E **91**, 012144 (2015).
[70] D. J. Luitz and Y. Bar Lev, Phys. Rev. Lett. **117**, 170404 (2016).
[71] R. Mondaini and M. Rigol, Phys. Rev. E **96**, 012157 (2017).
[72] D. Jansen, J. Stolpp, L. Vidmar, and F. Heidrich-Meisner, Phys. Rev. B **99**, 155130 (2019).